


Sandwich-like Nafion composite membrane with ultrathin ceria barriers for durable fuel cells

Yun Sik Kang¹ | Segeun Jang² | Eunho Choi² | Sunhee Jo³ |
Sang Moon Kim⁴ | Sung Jong Yoo^{5,6,7} 

¹Fuel Cell Laboratory, Korea Institute of Energy Research (KIER), Daejeon, Republic of Korea

²School of Mechanical Engineering, Kookmin University, Seoul, Republic of Korea

³Hydrogen Energy Business Development Team, Hyundai Motor Company, Uiwang-si, Republic of Korea

⁴Department of Mechanical Engineering, Incheon National University, Incheon, Republic of Korea

⁵Center for Hydrogen Fuel Cell Research, Korea Institute of Science and Technology (KIST), Seoul, Republic of Korea

⁶KHU-KIST Department of Converging Science and Technology, Kyung Hee University, Seoul, Republic of Korea

⁷Division of Energy & Environment Technology, KIST School, University of Science and Technology (UST), Daejeon, Republic of Korea

Correspondence

Sang Moon Kim, Department of Mechanical Engineering, Incheon National University, Incheon 22012, Republic of Korea.
Email: ksm7852@inu.ac.kr

Sung Jong Yoo, Center for Hydrogen Fuel Cell Research, Korea Institute of Science and Technology (KIST), Seoul 02792, Republic of Korea.
Email: ysj@kist.re.kr

Funding information

Korea Institute of Energy Technology Evaluation and Planning, Grant/Award Number: 20203020030010; National Research Foundation of Korea, Grant/Award Numbers: 2021M3H4A1A02042957, 2018M1A2A2061975, 2019R1C1C1004462

Summary

Improving the durability of the membrane electrode assembly (MEA) while obtaining high performance is required to further commercialize polymer electrolyte membrane fuel cells (PEMFCs). The durability of PEMFCs is improved by incorporating radical scavengers, such as CeO₂ (ceria), into the MEA, especially the membrane. However, nanosized ceria particles are generally mixed with ionomers and are cast on substrates to fabricate composite membranes. In such a case, controlling their morphology and avoiding particle agglomeration is difficult. Herein, we report a novel method for constructing a robust membrane by incorporating ultrathin ceria barriers into the outermost sides of a commercial Nafion membrane to effectively alleviate radical attacks while ensuring the high uniformity and controllability of ceria layers. The improved durability of the composite membrane is confirmed via ex situ Fenton's test and in situ operation of a fuel cell. Moreover, we observe that the amount of fluoride ion emission and the loss of proton conductivity of the membranes decrease as the CeO₂ density increases. The MEA comprises a modified membrane with CeO₂ barriers that show proper areal density. It demonstrates excellent durability under accelerated environmental conditions (open circuit voltage test) and acceptable initial performance with an insignificant decrease in proton conductivity.

KEYWORDS

chemical degradation, durability, membrane electrode assembly, polymer electrolyte membrane fuel cell, radical scavenger

Yun Sik Kang and Segeun Jang contributed equally to this study.

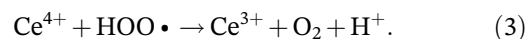
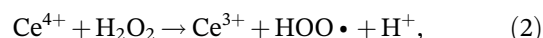
1 | INTRODUCTION

Polymer electrolyte membrane fuel cells (PEMFCs) have attracted attention as one of the most promising eco-friendly energy devices because of their high energy conversion efficiency and zero emission of pollutants, such as carbon dioxide, nitrogen oxides, sulfur oxides, or hydrocarbon materials.^{1,2} Given their several advantages, PEMFCs are considered a strong candidate as main power sources for automobile applications, such as hydrogen vehicles, portable devices, unmanned aerial vehicles, forklifts, excavators, or power generators for buildings.³⁻⁸ Membrane electrode assemblies (MEA) are the core part of PEMFCs because they serve as a site for electrochemical reactions. The MEA in PEMFCs comprises two catalyst layers (anode and cathode) and a proton exchange membrane.

Perfluorosulfonic acid (PFSA)-based membranes, such as Nafion, are commonly used for electrolytes in PEMFCs because of their high proton conductivity, flexible mechanical property, and structural stability.^{2,9,10} However, their high cost, high gas permeability, and chemical deterioration under harsh fuel cell operating conditions hinder the further commercialization of PEMFCs.^{11,12} During PEMFCs' operation at high current density, radicals such as hydroxyl (HO•), hydrogen (H•), or hydroperoxyl (HOO•) can be produced via an incomplete oxygen reduction reaction at the cathode or hydrogen gas crossover through the membrane. These radicals attack the perfluorocarbon backbone and sulfonic groups in the membrane or the ionomers in the catalyst layers and decompose the polymer backbone, resulting in the thinning of the membrane, dissolution of the bulk ionomers, and formation of defects on the surface.^{11,13-15} Consequently, the proton conductivities of the membrane and ionomers in the catalyst layers decrease considerably, and the gas crossover through the membrane increases, thereby reducing the open-circuit voltage (OCV), decreasing device performance, and shortening the lifetime of PEMFCs.

To mitigate the effects of radical attacks and reinforce the membrane, previous studies have incorporated radical scavengers or functional additives into the membrane.¹⁶⁻²⁵ The chemical stability of polymer membranes can be improved by introducing HO• radical scavengers, including organic chemical species, such as 3,4-dihydroxy-cinnamic acid and ClMe2SiH with carboxylic acids^{19,26,27}; inorganic nanoparticles, such as zirconium gadolinium oxide, titanium zirconium oxide, and cerium oxide²⁸⁻³⁰; and metal ions, such as cerium and manganese ions^{31,32} to the electrolyte membranes. Among the many types of radical scavengers, ceria (CeO₂) is commonly used because of its excellent radical

scavenging effect and regeneration property in highly acidic media via the oxidation–reduction (redox) reaction between Ce³⁺ and Ce⁴⁺ ionic states. Ceria has been considered as one of the most promising HO• radical scavengers because 1% of cerium ions with respect to sulfonic acid groups can quench 89% of HO• radicals, whereas 1% of manganese ions can scavenge 46% of these radicals. Such difference highlights the superior efficacy of cerium oxide relative to other metal oxides. The reaction between Ce³⁺ ions and HO• radicals in an acidic medium leads to the generation of Ce⁴⁺, as expressed in Equation (1). Meanwhile, Ce³⁺ can be regenerated via the reaction of Ce⁴⁺ ions with H₂O₂ or hydroperoxyl radicals during the cell operation, as shown in Equations (2) and (3). The cerium ions in cerium oxide exhibit radical scavenging behavior while bound in the oxide lattice.³³⁻³⁶



On the basis of these effects, CeO₂ has been applied to MEAs by introducing it to the membrane or catalyst layer to alleviate the chemical attacks of radicals.^{19,20,36,37} Although using CeO₂ in the MEA considerably increases the durability of PEMFCs, numerous technical issues still exist and include a significant decrease in the proton conductivity of membranes and ionomers, the blockage of the catalyst surface due to the aggregation of excess CeO₂ particles, and the dissolution of CeO₂ that can reduce the performance and durability of PEMFCs.^{38,39} In preparing CeO₂ containing a membrane, the ionomer solution and CeO₂ nanoparticles are mixed, and the resulting mixture is used to prepare the casting composite membrane.^{19,37} However, the fabrication of a robust membrane via the casting and control of the surface morphology is time-consuming and challenging.

To solve these technical issues and ensure the high stability and performance of MEAs, we propose a two-step process for fabricating CeO₂ nanoparticle layers at both sides of a commercial Nafion membrane. This process involves simple spin coating and thermal imprinting. In these processes, CeO₂ nanoparticle layers are prepared on a polyimide (PI) film via spin coating and are transferred to both sides of the membrane. This process differs from the conventional one in which ionomers and nanoparticles are mixed to form cast composite membranes. To effectively control radical attacks and prevent the blocking of the proton pathways at the membrane/electrode interface, the CeO₂ layers are placed on the

outermost sides of the Nafion membrane, where radical attacks commonly occur.^{14,40} Furthermore, because commercial Nafion membranes are used instead of the casting membrane in this study, several post-treatments can be excluded to achieve good physical properties for the membrane or CeO₂ aggregation tendency in the cast membrane. The CeO₂ layer coated Nafion membrane (CLCM) exhibits superior chemical stability relative to the conventional membrane, and the MEA with the CLCM shows enhanced device durability with minimal deterioration in PEMFC performance.

2 | EXPERIMENTAL SECTION

2.1 | Fabrication of Nafion membrane with CeO₂ layers on the front and back sides

CeO₂ solution (10 wt.% in H₂O) with <25 nm particle size was purchased from Sigma-Aldrich. The prepared CeO₂ solution was further diluted in H₂O to obtain CeO₂ solutions with concentrations of 1.0, 2.5, and 5.0 wt.%, which were sonicated for 30 minutes to effectively disperse the CeO₂ nanoparticles in H₂O. To form a well-dispersed thin CeO₂ layer, we dispensed small amounts of CeO₂ solutions with the three different concentrations of CeO₂ onto a PI film (50 μm, DuPont, United States) and treated the material with oxygen plasma (200 mTorr, 10 W). A syringe filter (1 μm filtration membrane, Whatman, United Kingdom) was used to prevent the aggregated CeO₂ particles from being dispensed. Then, the spin coating was performed at 3000 rpm for 2 minutes, and the CeO₂-coated PI film was oven-dried at ~80°C for 10 minutes to completely evaporate the remaining water. Next, Nafion 212 membrane (50 μm thickness, DuPont, United States) was placed between the CeO₂-coated PI films, and thermal imprinting was conducted at ~140°C for 3 minutes. After cooling down approximately to room temperature (RT), the sandwich-like assemblies were removed, and the PI films were gently peeled off from the Nafion membrane with CeO₂ layers on the front and back sides.

2.2 | Preparation of thin CeO₂ layer-embedded Nafion membrane

The thin Nafion membrane was fabricated by casting 5 wt.% Nafion solution containing lower aliphatic alcohols and water (Sigma-Aldrich, USA) onto a flat glass substrate placed on a hot plate at 80°C. After drying the solution on the hot plate for 5 hours, the Nafion-coated

glass was placed in a vacuum oven at 140°C and ~10 mTorr for 1 day. Next, the fabricated thin Nafion membrane with ~12 to 14 μm thickness was gently detached from the glass substrate. The process for embedding CeO₂ layers on both sides of the thin membrane was the same as that described previously.

2.3 | MEA and single-cell preparation

The MEAs were prepared as follows: The catalyst ink was prepared by mixing a carbon-supported platinum catalyst (40 wt.% Pt, Johnson Matthey, United Kingdom), distilled water, Nafion ionomer solution (5 wt.%, Sigma-Aldrich, United States), and 2-propanol (Sigma-Aldrich, United States) via sonication for ~20 minutes. Using a hand spray machine, the prepared catalyst ink was deposited on the Nafion membranes with and without CeO₂ layers on both sides with 0.12 mg cm⁻² Pt loading. The amount of Pt loadings of each sample was carefully checked by comparing the weight differences of the polyethylene terephthalate film before and after the spray coating of the Pt/C catalyst. During the deposition, the membranes were placed on a modified hot plate equipped with a vacuum pump to prevent swelling by quickly evaporating the solvent in the catalyst ink. The constructed catalyst-coated membranes were placed between the gas diffusion layers (39BC, SGL Carbon, Germany), and Teflon gaskets were inserted into the anode and cathode sides. The bipolar plates with graphite serpentine channels measuring ~1 mm in width and height were used as the flow field in a single cell. Each component was tightly assembled by fastening eight bolts by applying 80 ft lb. torque. The active geometric areas of the MEAs were set to 5.0 cm² for all samples.

2.4 | Electrochemical characterization

The polarization curves were measured using the PEMFC test system (CNL, Korea) with varying conditions. To measure the maximum performance of the single prepared cells, fully humidified H₂ (150 mL min⁻¹) and O₂ (200 mL min⁻¹) were supplied to the anode and cathode sides at ~70°C. After confirming the performance under humidified H₂/O₂ conditions with the current sweep method using a scan rate of 10 mA cm⁻² s⁻¹, the supplied O₂ gas at the cathode was replaced with humidified air (800 mL min⁻¹), and the performance of each sample was measured. The corresponding electrochemical impedance spectroscopy (EIS) spectra were measured using an impedance analyzer (HCP-803, Bio-Logic, France) at 0.6 V with a 10 mV AC disturbance.

The measurement frequency ranged from 0.1 Hz to 100 kHz, and other experimental conditions, including temperature and flow rates, were set to be the same as those for the polarization tests. A constant OCV and Fenton's tests were conducted to evaluate the chemical durability of the prepared membranes. For the constant OCV test, the cell temperature was maintained at 90°C by supplying partially humidified H₂ (300 mL min⁻¹) and O₂ (300 mL min⁻¹) with 35% relative humidity (RH), and OCV changes were recorded for 72 hours. For Fenton's test, the pristine Nafion membrane and the Nafion membranes with CeO₂ layers were immersed into a 30 mL Fenton solution (20 wt.% H₂O₂, 30 ppm Fe²⁺) at 80°C for 72 hours. Subsequently, the membranes were washed using deionized (DI) water, and the concentration of the fluoride ions in the Fenton solution was measured using an ion chromatography system (Orion Star A214, Thermo Scientific). The conductivities of the membranes before and after Fenton's test were measured using the AC impedance spectroscopic technique. The measurement was conducted in a frequency range of 0.1 Hz to 100 kHz under 1 mA AC at 70°C with 90% RH. The conductivity value was calculated using the following equation:

$$\sigma = \frac{L}{RA}, \quad (4)$$

where L (cm) is the distance between the working and reference electrodes, A (cm²) is the cross-sectional area of the membrane, and R is the membrane resistance calculated using the intercept of the semicircle on the EIS spectra with the real axis in the high-frequency range.^{41,42}

2.5 | Characterization

The existence of CeO₂ layers on the Nafion membrane was confirmed via X-ray diffraction (XRD) analysis (D/max2500/PC, Rigaku, Japan) with Cu-K α radiation source ($\lambda = 1.54 \text{ \AA}$). Fourier transform infrared (FT-IR) spectra were obtained to examine the chemical structures of the membranes. Nicolet-5700 FT-IR spectrometer (Thermo Electron Corporation, USA) equipped with an attenuated total reflectance (ATR) accessory was employed, and the spectra were recorded in the range of 4000 to 500 cm⁻¹ with a scan wavenumber of 5 cm⁻¹. The chemical compositions of the membranes before and after Fenton's test were measured using X-ray photoelectron spectroscopy (XPS) (Thermo VG Scientific, Germany) with consideration of K α radiation as the excitation source. Surface and cross-sectional

images of all prepared membranes were obtained via scanning electron microscopy (SEM) (Carl Zeiss, Germany), and transmission electron microscopy (TEM) images were obtained using FEI TITAN 80-300 transmission electron microscope operated at 200 kV. Thermogravimetric analysis (TGA) and differential scanning calorimetry (DSC) were conducted to confirm the thermal properties of the membranes. TGA was run from RT to 800°C under air atmosphere, and the heating rate was fixed to 5°C/min and DSC was recorded from RT to 550°C under the same atmosphere and heating rate.

3 | RESULTS AND DISCUSSION

3.1 | Fabrication of Nafion membrane with embedded CeO₂ layers

Figure 1A,B shows the fabrication of the Nafion membrane with ultrathin CeO₂ layers. The procedure comprised two main steps: First, well-dispersed CeO₂ nanoparticle layers were formed on a PI film via the spin coating process by using filtered CeO₂ nanoparticle (<25 nm) solution with three different concentrations dispersed in H₂O. Second, the CeO₂ layers were transferred from the PI film to the Nafion membrane via thermal imprinting at a temperature greater than the glass transition temperature (T_g) of the Nafion (~120°C) with ~1 MPa hydraulic pressure. The process was separated into two steps because the direct coating of the CeO₂ solution onto the Nafion membrane is made difficult by the swelling characteristic of the membrane and the CeO₂ nanoparticle layers can be easily incorporated into the Nafion membrane by using the hot-embossing method on the basis of the viscoelastic property of Nafion over T_g . Figure 1C shows the representative schematic of the completed Nafion membrane with CeO₂ layers. Figure S1 presents the digital camera images of the fabricated composite membranes with different CeO₂ concentrations. The ultrathin CeO₂ layers on the anode and cathode sides of the Nafion membrane were expected to effectively alleviate hydroxyl (HO•) and hydroperoxyl (HOO•) radical attacks at the forefront of the membrane.

3.2 | Characterizations of Nafion composite membrane with CeO₂ layers

Figure 2A shows the TEM image of the CeO₂ nanoparticles with a size of ~25 nm. The corresponding energy dispersive X-ray (EDX) analysis further confirmed

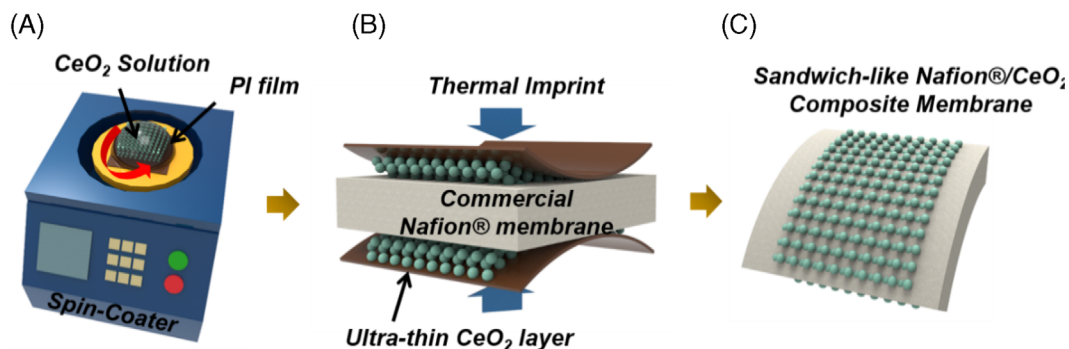


FIGURE 1 Schematic illustrations of preparation of Nafion membrane with ultrathin CeO_2 layers. (A) Formation of well-dispersed CeO_2 nanoparticle layers on PI film via spin coating. (B) Transfer of CeO_2 layers from PI film to Nafion membrane via thermal imprinting. (C) Constructed composite Nafion membrane with embedded CeO_2 layers

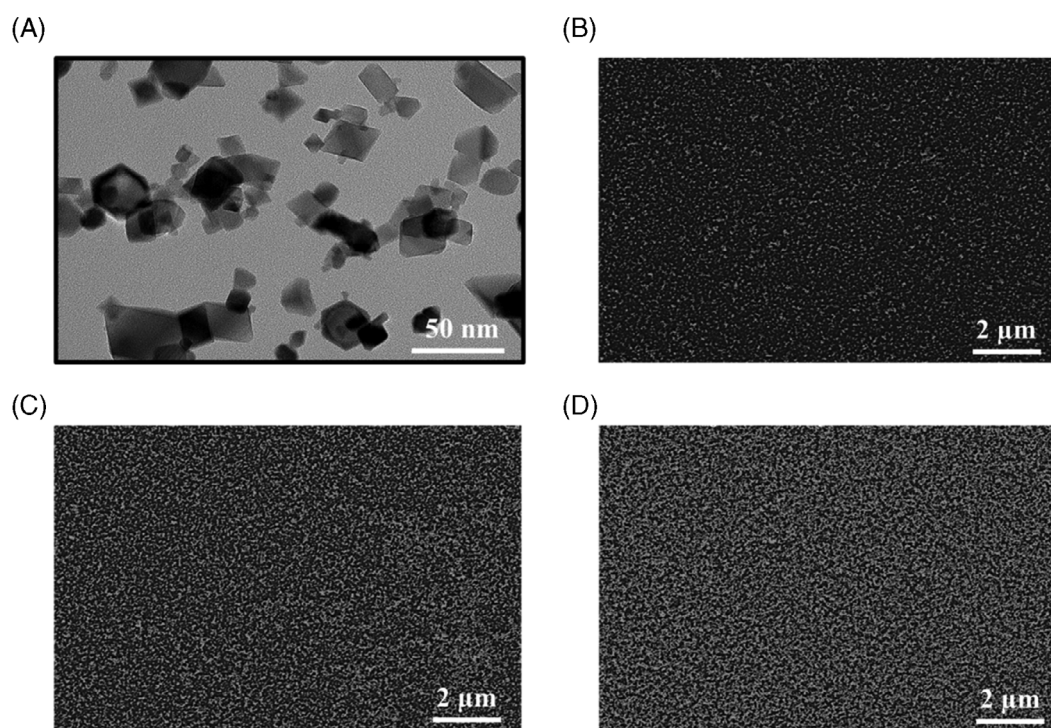


FIGURE 2 (A) TEM image of CeO_2 nanoparticles. Top-view SEM images of CeO_2 -coated PI film with (B) 1.0 wt.%, (C) 2.5 wt.%, and (D) 5.0 wt.% CeO_2 solution

the elemental constituents and atomic wt.% of the CeO_2 nanoparticles (Figure S2). The particle size was carefully selected on the basis of previous studies.^{39,43} The active surface area of ceria particles would be inversely proportional to the particle size, and the scavenging effect was expected to be enhanced using smaller-sized particles. However, extremely fine particles, often with sizes below 10 nm, tend to be intensively agglomerated because of the weak repulsive forces between particles and their inherent instability.⁴⁴ Moreover, the chemical stability of ceria nanoparticles reportedly increases with increased crystallite size and decreased surface area per unit

mass.³⁹ Hence, particles with suitably large sizes should be used to achieve high effectiveness and acceptable stability. In other words, the scavenging effect of hydroxyl radicals is more effective for larger nanoparticles (>10 nm) than for small-sized nanoparticles (~4–6 nm), which exhibit a pronounced agglomeration problem. Herein, CeO_2 nanoparticle agglomeration in the solutions was prevented using a syringe filter with a 1 μm filtration membrane, and the spin coating process with high rotational speed (~3000 rpm) led to the formation of well-distributed CeO_2 layers on the oxygen plasma-treated hydrophilic PI films (Figure 2B–D). As the concentration

of the CeO_2 solution increased from 1.0 to 5.0 wt.%, the density of the coated CeO_2 region increased proportionally, thereby indicating that the coated layer characteristics could be easily controlled by simply modifying the concentration of the CeO_2 solution.

Relative to other coating methods, including slot die and bar coating, which use viscous slurry and are challenging to use in attaining sub-micrometer films without particle agglomeration, the spin coating method gives a great advantage in the uniform and effective distribution of particles by using a high centrifugal force with a diluted solution and avoiding the coffee ring effect induced particle agglomeration. Cross-sectional SEM images were obtained to check the thickness of the coated CeO_2 layers (Figure S3). Unlike the coating density trend, which is proportional to the solution concentration, the thicknesses of the samples were almost similar (~ 50 – 80 nm), corresponding to two or three layers of CeO_2 nanoparticles. The thickness and surface coverage of CeO_2 in the spin coating being dependent on different solution concentrations are discussed in the Data S1 section. The Nafion membranes with embedded CeO_2 layers were characterized after confirming the morphological characteristics of the CeO_2 layers after spin coating. Figure 3A shows the SEM images in the backscattered electron (BSE) mode of the cross-sectional Nafion/ CeO_2

layer composite membrane with 2.5 wt.% CeO_2 solution. The CeO_2 layers were successfully embedded into the Nafion membrane surface, as further confirmed by the magnified cross-sectional SEM images in Figure S4. In addition, the XRD analysis verified the existence of CeO_2 layers in the Nafion composite membrane (Figure S5).

To address the bulk physical properties of the ceria-embedded Nafion composite membrane, we conducted a tensile test. We expected that the overall mechanical properties of the Nafion membrane would not be greatly affected because the loading amount of ceria was considerably smaller than that of Nafion. As expected, the tensile stress and elongation at the break value were comparable (Figure 4), thereby indicating that the embedded ceria did not act as a physical defect site on the membrane. However, we observed that the water uptake increased as the amount of loaded CeO_2 increased because of the water retention effect induced by the hygroscopic property of CeO_2 . The measured values are summarized in Table 1.

The FT-IR spectra of the Nafion 212 membrane and ceria-modified Nafion membranes were obtained in the range of 500 – 4000 cm^{-1} in ATR mode to identify the chemical structures of the samples. Figure 5 shows that both spectra had identical peaks corresponding to the Nafion structure (peak at 1060 cm^{-1} due to symmetric

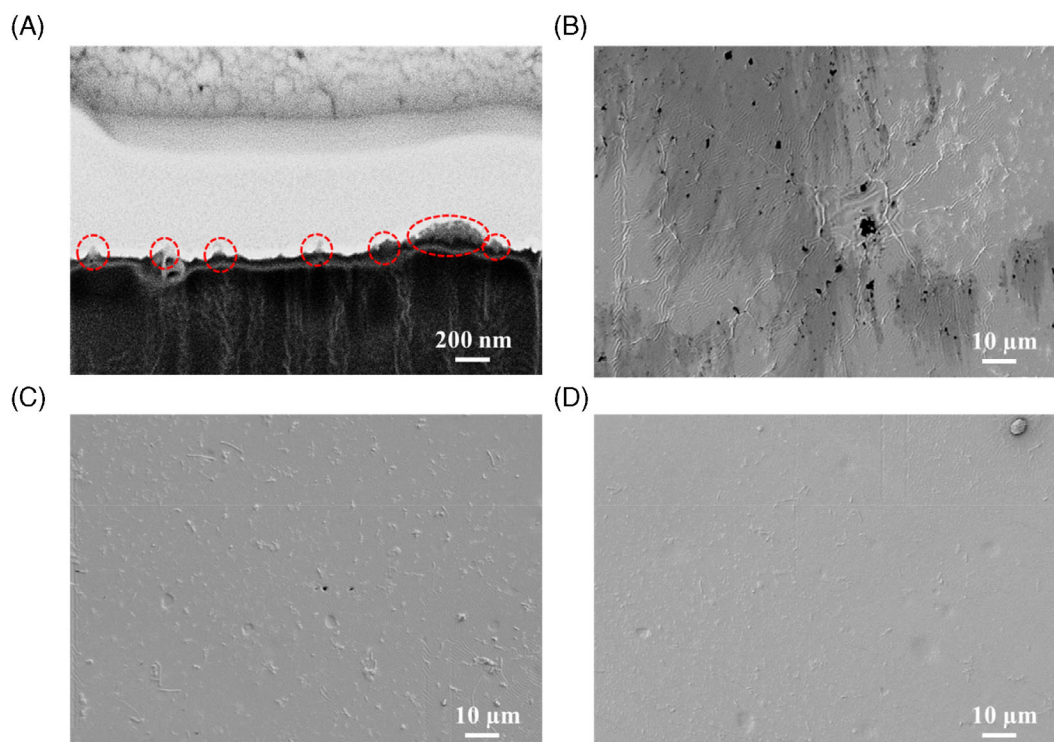


FIGURE 3 (A) SEM images of cross-sectional Nafion/ CeO_2 layer composite membrane with 2.5 wt.% CeO_2 solution in BSE mode. Surface SEM images of (B) commercial Nafion 212 membrane, (C) Nafion 212 membrane with CeO_2 layers of 1.0 wt.% solution, and (D) Nafion 212 membrane with CeO_2 layers of 2.5 wt.% solution after Fenton's test

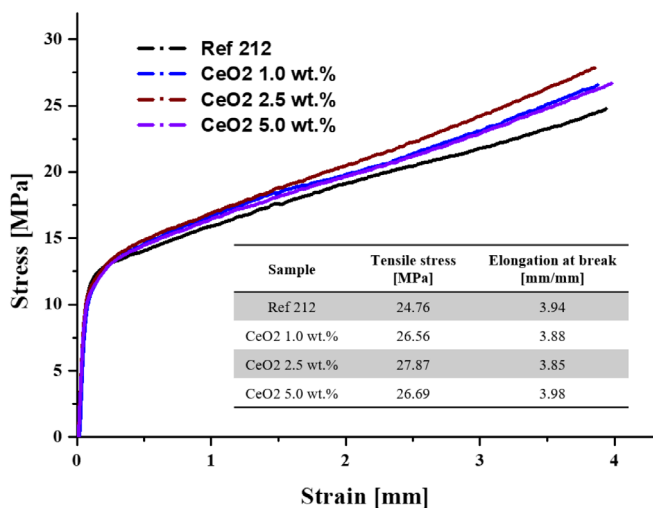


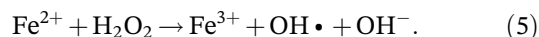
FIGURE 4 Measured stress–strain curves for pristine membrane and ceria-embedded membranes through tensile test

S–O stretching, peak at 1150 cm^{-1} due to symmetric C–F stretching, peak at 1204 cm^{-1} due to asymmetric C–F stretching, peak at 3460 cm^{-1} due to –H stretching vibration by physically adsorbed water, and peak at 1600 to 1800 cm^{-1} due to O–H bending vibration of free water molecules).^{45–47} The ceria particles were transferred to the surface of a commercially premade Nafion membrane through thermal imprinting with the use of the dispersed CeO₂ nanoparticles on the PI film. This method is different from the conventional casting and drying method for making composite membranes because of the use of the mixed solution of cerium ions and Nafion ionomers. Therefore, the ceria particles were physically embedded on the membrane surface by retaining their original shape as dispersive. These particles did not affect the polymeric chemical structure of the Nafion membrane. The only difference was that the intensity of the ceria-coated Nafion membrane at 1600 to 1800 cm^{-1} increased because of the hydrophilicity of the oxide nanoparticles on the surface.⁴⁶

We also measured the TGA and DSC for the bare Nafion membrane and composite membrane to confirm their thermal properties (Figures 6 and 7, respectively). In the TGA results, the pure Nafion membrane apparently experienced decomposition from $\sim 300^\circ\text{C}$ and rapidly decomposed in the range of 450 to 550°C . Meanwhile, the composite membrane showed different TGA curves near ~ 300 and $\sim 500^\circ\text{C}$ possibly because of the effect of the ceria nanoparticles or the decomposition of organic compounds in the ceria dispersion used.^{48,49} The left shift of the curves of the CeO₂-coated Nafion membrane, relative to those of the pristine Nafion membrane near 300°C , could be attributed to the decomposition of the organic compounds used for ceria dispersion.

The right shift of the curve near 500°C was ascribed to the remaining CeO₂ particles even with high temperatures. However, the intensity difference of the signals between the ceria composite membranes was very small because of the fact that the contribution of the mass of the embedded ceria was very minimal. Moreover, the DSC results of the samples showed that the ceria-coated Nafion membrane had the same thermal properties as Nafion, except for the negative shifting of the peaks at ~ 300 to 330°C and the increased amount of heat flow (peak integration) resulting from the existence of ceria nanoparticles; these results showed a good agreement with the TGA outcomes.⁵⁰

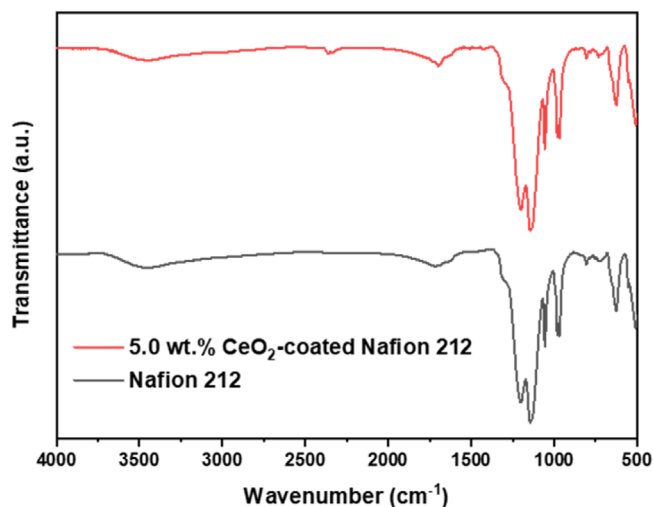
To evaluate the radical scavenging effect of the Nafion membrane with CeO₂ layers, ex situ Fenton's test was conducted. Commercial Nafion 212 membrane and the modified Nafion 212 membrane with CeO₂ layers with different coating densities were immersed in a Fenton solution (20 wt.% H₂O₂, 30 ppm Fe²⁺) at 80°C for 72 hours. Hydroxyl radicals (OH•) were generated via this process as follows^{51–53}:



Thereafter, the membranes were washed using DI water, and the characterizations were conducted to observe the physicochemical changes of the membrane before and after Fenton's test. Figure 3B–D shows the surface SEM images of the commercial Nafion 212 membrane, Nafion 212 membrane with CeO₂ layers of 1.0 wt.% solution, and Nafion 212 membrane with CeO₂ layers of 2.5 wt.% solutions. Numerous defects of the commercial Nafion 212 membrane were observed after conducting Fenton's test, and they were attributed to chemical degradation from radical attacks. However, the modified commercial Nafion membrane with CeO₂ layers showed relatively few defects. This result indicated that the ultrathin CeO₂ layers at the forefront of the membrane could effectively alleviate the membrane degradation from radical attacks. To quantitatively investigate the radical scavenging effect of the CeO₂ layers, we checked the amount of fluoride ion emission during Fenton's test. The results indicated the chemical degradation of the PFSA Nafion membrane. Relative to that for the commercial membrane, the amount of fluoride ion emission for the modified membrane with CeO₂ layers was sufficiently reduced (Figure 8A). Furthermore, the proton conductivity measurements of each membrane before and after Fenton's test indicated that as the areal density of the CeO₂ nanoparticles on the membrane increased, the radical attack on the membrane decreased, thus alleviating degradation and conductivity loss (Figure 8B).

TABLE 1 Dimensional change and water uptake of pristine membrane and ceria-embedded membranes

Samples	Length change (x-axis) (%)	Length change (y-axis) (%)	Thickness change (z-axis) (%)	Water uptake (%)
Reference MEA	15	15	20.4	22.7
CeO ₂ 1.0 wt.%	15	12.5	23.4	24.7
CeO ₂ 2.5 wt.%	15	12.5	24.5	27.3
CeO ₂ 5.0 wt.%	15	12.5	25	31.2

FIGURE 5 FT-IR spectra of Nafion 212 and Nafion 212 membrane with 5.0 wt.% CeO₂

To compare the chemical compositions of the membranes before and after Fenton's test, we obtained and analyzed the XPS results.⁵⁴⁻⁵⁹ Figure 9 shows the C 1s XPS spectra of the membranes. To quantitatively analyze the effect of the CeO₂ layers on the membranes as a radical scavenger, we deconvoluted the C 1s signal into five peaks: CF₂ (291.6 eV), terminal CF₃ groups (293.3 eV), O=C—O (289.3 eV), C—O (286.4 eV), and C—H/C=C (284.4 eV). Before Fenton's test, the peaks of all the measured spectra represented the four environments of the main chemical constituents of the Nafion membrane, namely, C—F₂, C—F₃, C—S, and C—O bonds, with little difference in the spectra taken from each sample. After conducting Fenton's test, all samples showed a significant decrease in the peak intensity of CF₂ (at 291.6 eV) and an increase in the peak intensities of the COOH and C—H bonds (at 289.4 and 284.4 eV, respectively). These effects were associated with the chemical degradation of the Nafion membrane. In addition, the decrease in the intensity for S 2p and F 1s after Fenton's test can be attributed to the polymer decomposition (Figure S6).

According to the XPS results, the possible chemical degradation mechanisms of the Nafion membrane during

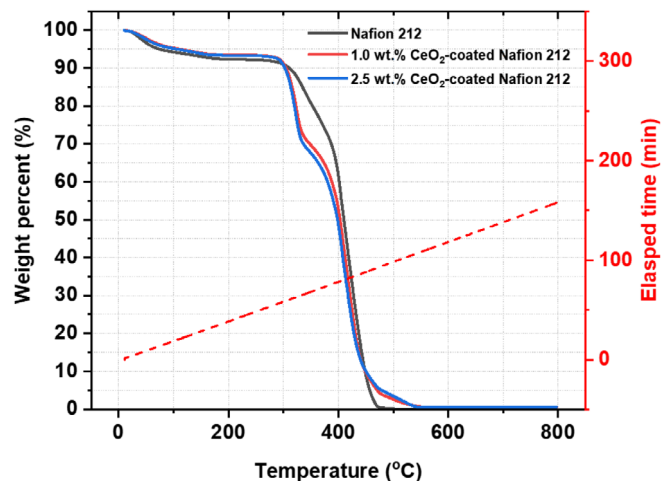


FIGURE 6 Thermogravimetric analysis (TGA) for pristine membrane and ceria-embedded membranes

Fenton's test are as follows: (a) When the COOH at the end of the Nafion polymer is attacked by an OH radical, it is decomposed into CO₂ and HF, hence the gradual shortening of the polymer backbone. (b) When the C—S bond is attacked by an OH radical, the SO₃⁻ group is lost, and the side chain is decomposed. (c) When the carbon atom connecting the polymer backbone and the side chain is attacked, side chains and two backbones are formed, and their ends form COOH. The deterioration processes of the Nafion membrane share a similarity—the formation of COOH following the decomposition of (CF₂)_n polymers. Moreover, the hydrocarbon contamination on the membrane surface may be due to decomposed polymers. The peak intensity increased at 284.4 eV and indicated surface deformation by degraded polymers. As indicated by the comparison of the XPS peak areas of CF₂ of the membranes before and after Fenton's test, the Nafion membrane decomposition occurred slowly as the CeO₂ content increased. For the pristine Nafion membrane, only 49.8% of the polymer backbones were maintained. For the Nafion membrane with 2.5 wt.% CeO₂, ~62.5% of the polymer backbones were maintained. The XPS results showed that the CeO₂

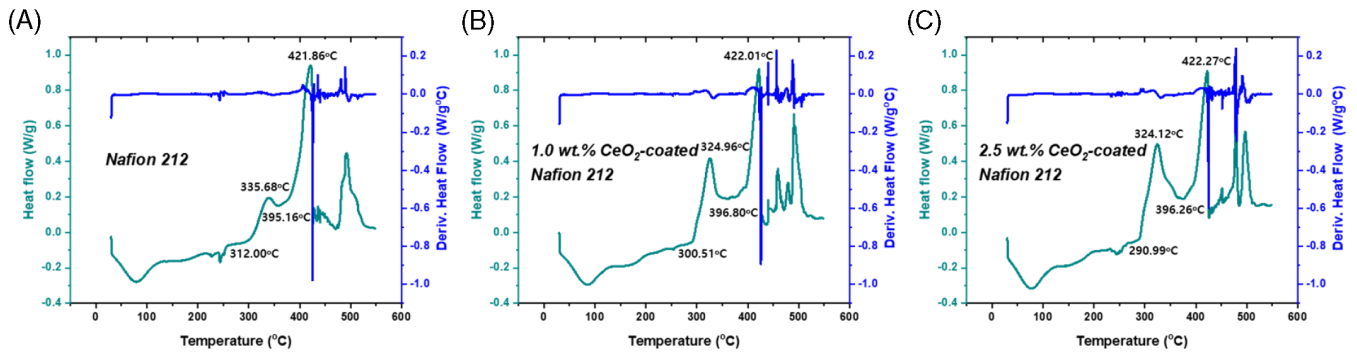


FIGURE 7 Differential scanning calorimetry (DSC) results for pristine membrane and ceria-embedded membranes

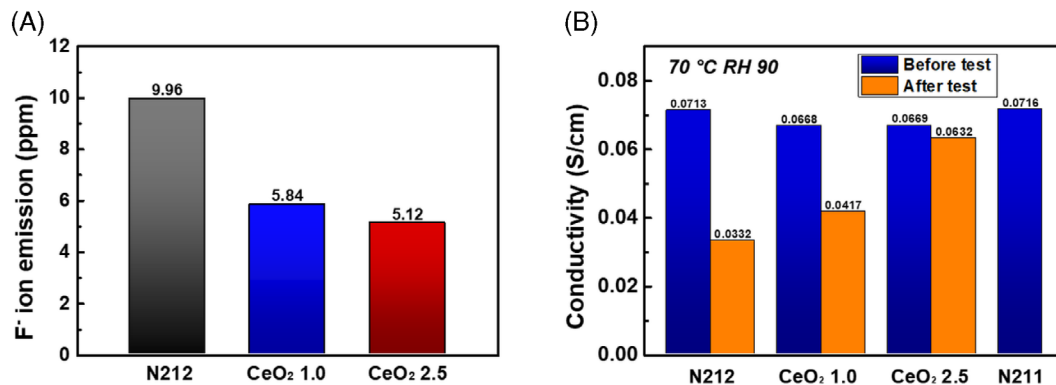


FIGURE 8 (A) Graph of fluoride ion emission of membrane after Fenton's test. (B) Proton conductivity change of each membrane before and after Fenton's test

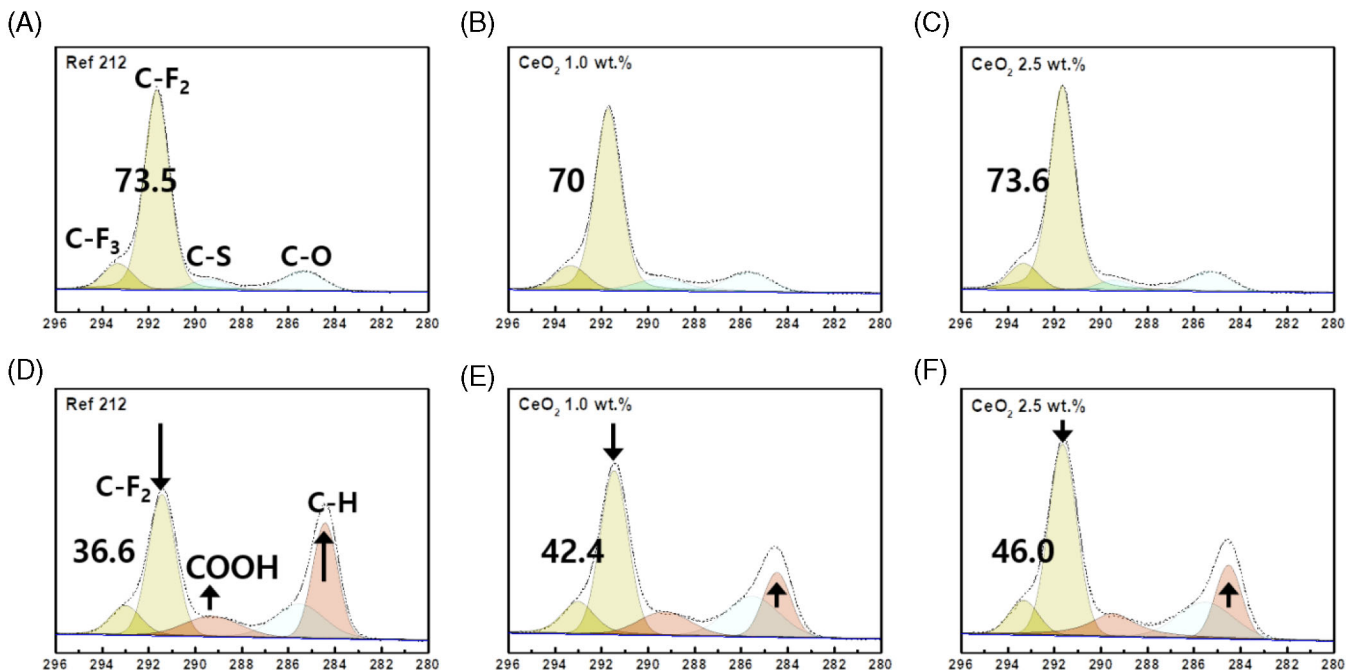


FIGURE 9 XPS C 1s spectra of the membranes before and after Fenton's test. (A), (D) Nafion 212; (B), (E) membrane with 1.0 wt.% CeO_2 ; and (C), (F) membrane with 2.5 wt.% CeO_2

layers considerably improved the chemical durability of the Nafion membrane.

We obtained the SEM images and EDS spectra of the 5.0 wt.% of ceria-coated Nafion membrane before and after the treatment to confirm the changes in the surface morphology and chemical composition. Figure S7 shows that although the ceria nanoparticles on the surface disappeared in many parts after 72 hours of Fenton's reaction in harsh conditions, they remained on the surface of the ceria-coated membrane without any defects.

3.3 | Fuel cell performance

To confirm the effect of the CeO₂ layer of the Nafion composite membrane, single cells were constructed using pristine Nafion 212 and Nafion membranes with 1.0 and 2.5 wt.% CeO₂ nanoparticle layers, respectively. A 72 hours OCV test was conducted (Figure 10A). The OCV of the samples before the test was more than 0.95 V, which indicated that the PEMFCs were effectively polarized by the membranes and were established well. However, with the increase in the retention time at the OCV state, the OCV of the PEMFCs gradually decreased because of the damage to the Nafion membrane. In the comparison of the pristine PEMFC and the PEMFCs with

CeO₂ layers, the latter showed better chemical durability, whereas the PEMFC with 2.5 wt.% CeO₂ showed only a 72 mV reduction in the OCV value even after conducting the 72 hours test (124 and 93 mV for the PEMFCs without and with 1.0 wt.% CeO₂, respectively). The OCV test results confirmed that the CeO₂ layers significantly improved the chemical durability of the Nafion membrane. The performances of the PEMFCs were compared before and after the OCV test. Fully humidified H₂/O₂ (or Air) gases were supplied to the anode/cathode of the PEMFCs, and the operating temperature was fixed at 70°C. Before the OCV test, as the CeO₂ loading increased from 0 to 2.5 wt.%, the maximum power densities of the PEMFCs decreased owing to the decreased proton conductivity, which resulted in increased ohmic resistance (Figure 10B,C). However, after the OCV test, the order of the PEMFCs' performance was completely reversed, especially at the H₂/Air operation condition. The maximum power densities of the PEMFCs before and after the OCV test are provided in Table 2.

Notably, the PEMFC with a membrane having 2.5 wt.% CeO₂ showed almost zero reduction in performance before and after the OCV test. The result indicated that as the loading of radical scavengers in membranes increases, the chemical durability can be considerably improved. However, if the amount of radical scavengers exceeds the

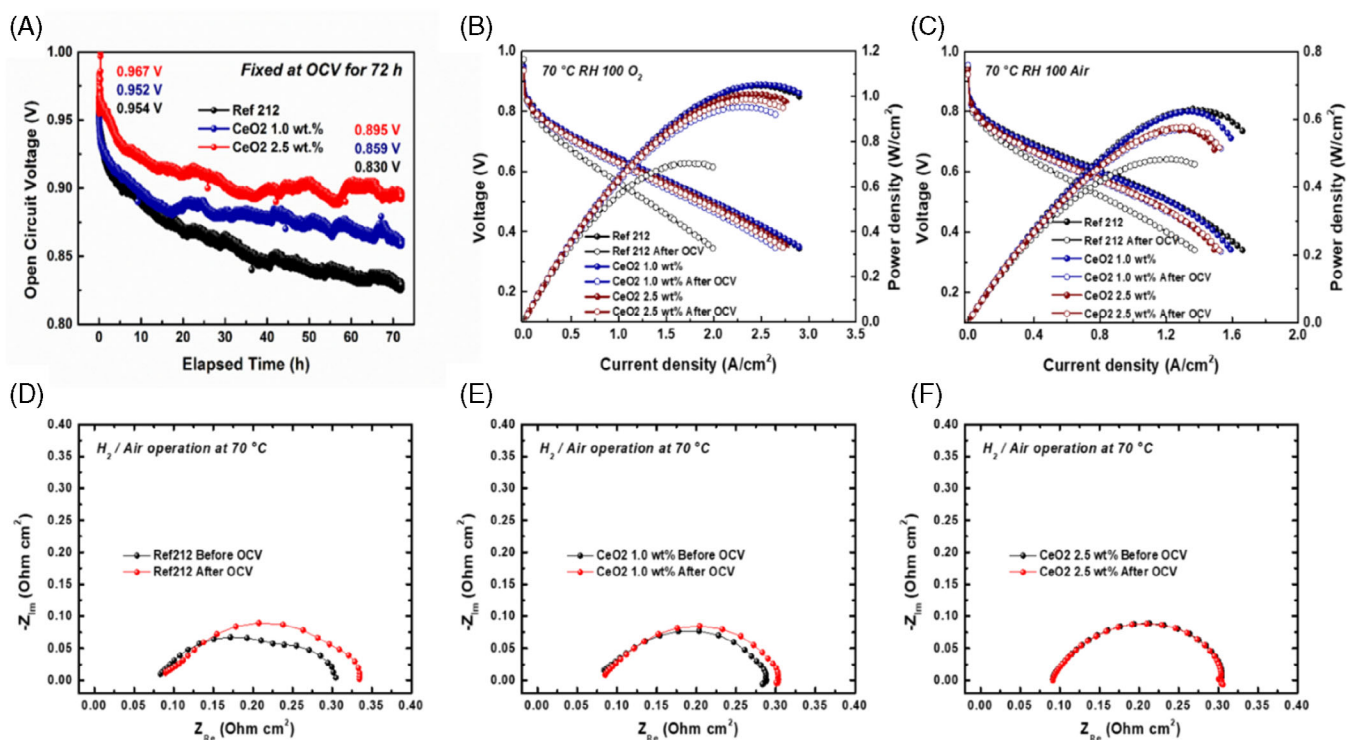


FIGURE 10 (A) OCV profiles of MEAs with OCV retention for 72 hours. Polarization curves of MEAs with various CeO₂ loadings before and after OCV test with (B) H₂/O₂ and (C) H₂/Air operations. EIS spectra of MEAs with (D) Nafion 212, (E) 1.0 wt.% CeO₂, and (F) 2.5 wt.% CeO₂ before and after OCV test

TABLE 2 Maximum power densities of PEMFCs before and after OCV test

Membrane	Maximum power densities at H ₂ /O ₂ operation (W cm ⁻²)		Maximum power densities at H ₂ /Air operation (W cm ⁻²)	
	Before OCV	After OCV	Before OCV	After OCV
Reference MEA	1.050	0.704	0.631	0.482
MEA with 1.0 wt.% of CeO ₂	1.051	0.958	0.623	0.571
MEA with 2.5 wt.% of CeO ₂	1.012	0.992	0.574	0.577

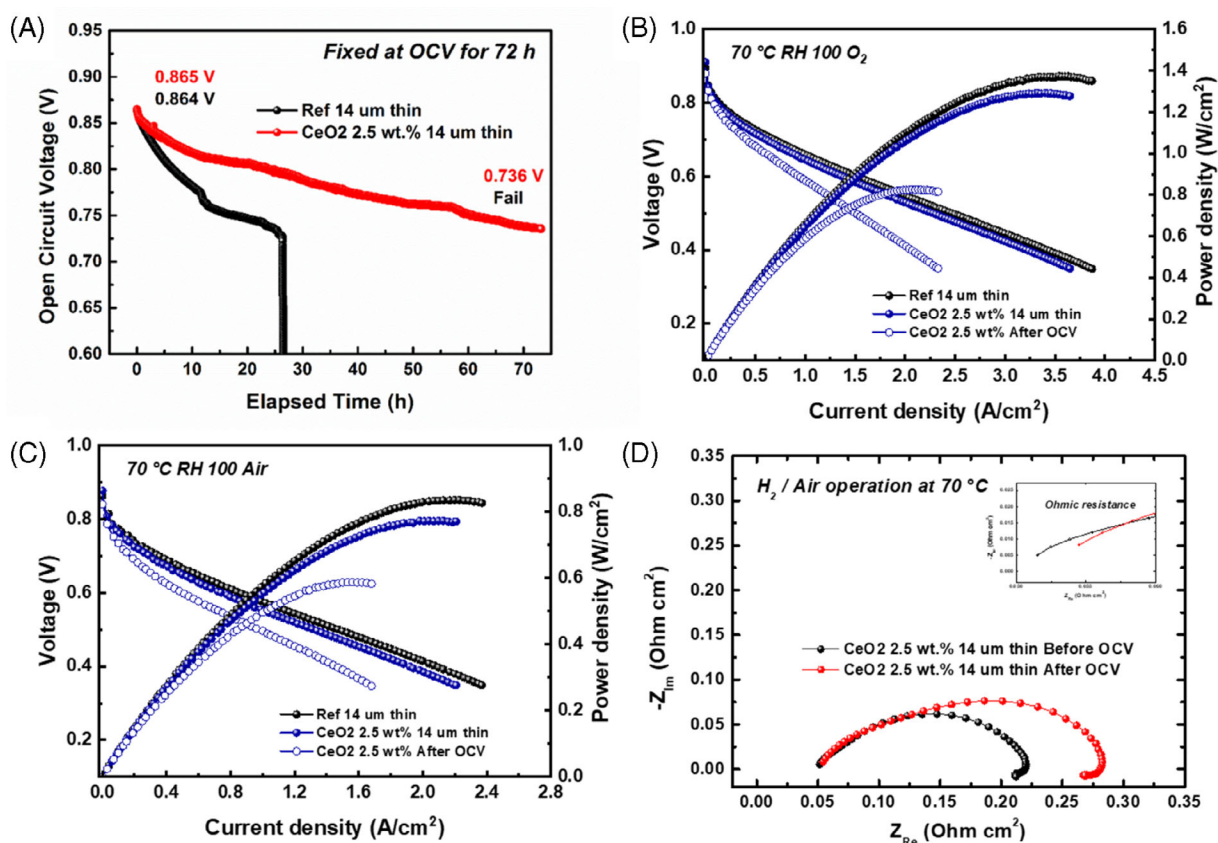


FIGURE 11 (A) OCV profiles of MEAs having thin membranes with OCV retention for 72 hours. Polarization curves of MEAs with thin membranes before and after OCV test with (B) H₂/O₂ and (C) H₂/Air operations. (D) EIS spectra of MEAs having thin membranes with 2.5 wt.% CeO₂ before and after OCV test

proper level, then the fuel cell performance could deteriorate. The EIS spectra of the samples at H₂/Air operation conditions were also measured (Figure 10D–F). The results of the comparison of the ohmic (R_{ohm}) and charge transfer (R_{ct}) resistances of the PEMFCs agreed with the polarization test results, that is, with the increase in CeO₂ loading, the increase in R_{ohm} and R_{ct} before and after the test is reduced. To ensure the effectiveness of the ceria-embedded composite membrane in the inhibition of pinhole formation, we measured the hydrogen crossover current densities of the samples before and after the OCV test through linear sweep voltammetry (LSV). The hydrogen crossover current density of the bare Nafion membrane after the OCV test

dramatically increased relative to that of the membrane before the OCV test. Meanwhile, the ceria-embedded composite membrane exhibited no significant increment in hydrogen crossover current after the OCV test (Figure S8 and Table S1). The result indicated that the embedded ceria on the membrane acted as a highly effective radical scavenger and inhibited pinhole formation on the membrane.

Figure S9 shows an extremely thin membrane with $\sim 14 \mu\text{m}$ thickness that was prepared via ionomer solution casting to investigate the effects of the CeO₂ layers on the chemical durability of the cast membrane and the constructed MEA. A thin membrane containing CeO₂ layers was also prepared using the same process as that

for the commercial Nafion membrane with CeO₂ layers. OCV tests were conducted as well. Figure 11A shows that the PEMFC with the thin membrane of ~14 μm without the CeO₂ layer was severely damaged after 26 hours, resulting in a sharp OCV decrement. Furthermore, the PEMFC performance could not be measured after conducting the OCV test. The digital camera images of the MEAs showed that pinholes were generated on the MEAs (Figure S10). Meanwhile, the PEMFC with the thin membrane containing CeO₂ layers maintained the OCV values, and the PEMFC performance was smoothly measured even after the 72 hours OCV test (Figure 11A–C), even though R_{ohm} and R_{ct} of the PEMFC increased in the EIS spectra (Figure 11D). The results of these thin membrane samples clearly showed that the CeO₂ layers improved the chemical durability of the membranes.

An MEA with 5.0 wt.% CeO₂ layer was prepared to confirm the effect of CeO₂ loading on the fuel cell performance and chemical durability. An MEA with a CeO₂ layer was also fabricated in the same manner (Figure S11), and the polarization curves were measured using fully humidified H₂/O₂ (or Air) gases at 70°C (Figure S12a). The OCV holding test was also performed (Figure S12b). Although we confirmed that the high loading of CeO₂ increased the chemical durability of the MEA, excessive radical scavengers (high areal density of ceria layers) in the MEA could act as interfacial resistance and thus considerably reduce device performance. Therefore, the optimal loading of radical scavengers (proper areal density) should be used in the MEA to simultaneously establish acceptable device performance and durability.

4 | CONCLUSION

In this study, well-distributed CeO₂ layers were incorporated on both sides of an electrolyte membrane to enhance the durability of MEAs in fuel cells. The solutions containing CeO₂ particles with sizes <25 nm were prepared using different concentrations (1.0, 2.5, and 5.0 wt.%), and each solution was spin-coated on the plasma-treated PI film used for transferring the CeO₂ substrate to the Nafion membrane surfaces. The CeO₂ layers were uniformly distributed on the substrate with two or three layers regardless of the solution concentration. In addition, the areal density of the CeO₂ particles on the substrate was proportional to the concentrations of the solutions. The CeO₂ layer-embedded commercial Nafion membrane showed a satisfactory scavenging effect from radical attacks at the forefront of the membrane, as confirmed via ex situ Fenton's test and in situ OCV

holding test. Although a large number of radical scavengers (high areal density of ceria layers) showed excellent radical scavenging ability, they also acted as interfacial resistance, thus reducing device performance. The MEA with a modified membrane that was constructed using optimal ceria barriers (2.5 wt.% CeO₂ solutions) showed significantly improved chemical durability and acceptable initial performance with an insignificant decrease in proton conductivity relative to the MEA with conventional membrane. This novel methodology of constructing CeO₂ layers with proper areal density on both sides of a membrane can be an effective approach to improving the durability of fuel cells.

ACKNOWLEDGEMENTS

This work was supported by the National Research Foundation of Korea (Grant Nos. 2018M1A2A2061975, 2019R1C1C1004462, 2021M3H4A1A02042957) and the KIST Institutional Program and by the New & Renewable Energy Core Technology Program of KETEP (20203020030010) in Korea.

ORCID

Sung Jong Yoo  <https://orcid.org/0000-0003-0238-5971>

REFERENCES

1. Gasteiger HA, Marković NM. Just a dream—or future reality? *Science*. 2009;324(5923):48-49.
2. O'hayre R, Cha S-W, Colella W, Prinz FB. *Fuel cell fundamentals*. Hoboken, NJ: John Wiley & Sons; 2016.
3. Dyer CK. Fuel cells for portable applications. *J Power Sources*. 2002;106(1–2):31-34.
4. Paulson LD. Industry trends - will fuel cells replace batteries in mobile devices? *Computer*. 2003;36(11):10-12.
5. Kim K, Kim T, Lee K, Kwon S. Fuel cell system with sodium borohydride as hydrogen source for unmanned aerial vehicles. *J Power Sources*. 2011;196(21):9069-9075.
6. McConnell VP. Military UAVs claiming the skies with fuel cell power. *Fuel Cells Bull*. 2007;2007(12):12-15.
7. Keränen TM, Karimäki H, Viitakangas J, et al. Development of integrated fuel cell hybrid power source for electric forklift. *J Power Sources*. 2011;196(21):9058-9068.
8. Li T, Huang L, Liu H. Energy management and economic analysis for a fuel cell supercapacitor excavator. *Energy*. 2019;172:840-851.
9. Spiegel C. *Designing and building fuel cells*, Vol 87. New York City, NY: McGraw Hill; 2007.
10. Kusoglu A, Weber AZ. New insights into perfluorinated sulfonic-acid ionomers. *Chem Rev*. 2017;117(3):987-1104.
11. Wong KH, Kjeang E. Macroscopic in-situ modeling of chemical membrane degradation in polymer electrolyte fuel cells. *J Electrochem Soc*. 2014;161(9):F823-F832.
12. Chandresris M, Vincent R, Guetaz L, Roch JS, Thoby D, Quinaud M. Membrane degradation in PEM fuel cells: From experimental results to semi-empirical degradation laws. *Int J Hydrogen Energy*. 2017;42(12):8139-8149.

13. Yoon W, Fundamental study of mechanical and chemical degradation mechanisms of PEM fuel cell membranes. Ph.D. dissertation. 2010. University of Central Florida
14. Ramaswamy N, Hakim N, Mukerjee S. Degradation mechanism study of perfluorinated proton exchange membrane under fuel cell operating conditions. *Electrochim Acta*. 2008; 53(8):3279-3295.
15. Frühwirt P, Kregar A, Törring JT, Katrašnik T, Gescheidt G. Holistic approach to chemical degradation of nafion membranes in fuel cells: Modelling and predictions. *Phys Chem Chem Phys*. 2020;22(10):5647-5666.
16. D'Urso C, Oldani C, Baglio V, Merlo L, Aricò AS. Towards fuel cell membranes with improved lifetime: Aquivion® perfluorosulfonic acid membranes containing immobilized radical scavengers. *J Power Sources*. 2014;272:753-758.
17. Wang Z, Tang H, Zhang H, et al. Synthesis of nafion/CeO₂ hybrid for chemically durable proton exchange membrane of fuel cell. *J Membr Sci*. 2012;421-422:201-210.
18. Taghizadeh MT, Vatanparast M. Ultrasonic-assisted synthesis of ZrO₂ nanoparticles and their application to improve the chemical stability of nafion membrane in proton exchange membrane (PEM) fuel cells. *J Colloid Interface Sci*. 2016;483: 1-10.
19. Park Y, Kim D. Chemical stability enhancement of nafion membrane by impregnation of a novel organic-OH radical scavenger, 3, 4-dihydroxy-cinnamic acid. *J Membr Sci*. 2018; 566:1-7.
20. Baker AM, Wang L, Johnson WB, Prasad AK, Advani SG. Nafion membranes reinforced with ceria-coated multiwall carbon nanotubes for improved mechanical and chemical durability in polymer electrolyte membrane fuel cells. *J Phys Chem C*. 2014;118(46):26796-26802.
21. Kim AR, Gabunada JC, Yoo DJ. Amelioration in physicochemical properties and single cell performance of sulfonated poly (ether ether ketone) block copolymer composite membrane using sulfonated carbon nanotubes for intermediate humidity fuel cells. *Int J Energy Res*. 2019;43(7):2974-2989.
22. Kim AR, Vinothkannan M, Song MH, Lee JY, Lee HK, Yoo DJ. Amine functionalized carbon nanotube (ACNT) filled in sulfonated poly (ether ether ketone) membrane: effects of ACNT in improving polymer electrolyte fuel cell performance under reduced relative humidity. *Compos Part B Eng*. 2020;188: 107890.
23. Vinothkannan M, Ramakrishnan S, Kim AR, Lee HK, Yoo DJ. Ceria stabilized by titanium carbide as a sustainable filler in the nafion matrix improves the mechanical integrity, electrochemical durability, and hydrogen impermeability of proton-exchange membrane fuel cells: effects of the filler content. *ACS Appl Mater Interf*. 2020;12(5):5704-5716.
24. Vinothkannan M, Hariprasad R, Ramakrishnan S, Kim AR, Yoo DJ. Potential bifunctional filler (CeO₂-ACNTs) for nafion matrix toward extended electrochemical power density and durability in proton-exchange membrane fuel cells operating at reduced relative humidity. *ACS Sustain Chem Eng*. 2019;7(15): 12847-12857.
25. Vinothkannan M, Kim AR, Yoo DJ. Potential carbon nanomaterials as additives for state-of-the-art nafion electrolyte in proton-exchange membrane fuel cells: a concise review. *RSC Adv*. 2021;11(30):18351-18370.
26. Babu SA, Yasuda M, Baba A. Mediated chemoselective dehydrogenative interaction of CIME2SiH with carboxylic acids: direct chemo- and regioselective Friedel-Crafts acylation of aromatic ethers. *Org Lett*. 2007;9(3):405-408.
27. Kim K, Bae J, Lim M-Y, et al. Enhanced physical stability and chemical durability of sulfonated poly (arylene ether sulfone) composite membranes having antioxidant grafted graphene oxide for polymer electrolyte membrane fuel cell applications. *J Membr Sci*. 2017;525:125-134.
28. Han D, Hossain SI, Son B, Lee DH, Shanmugam S. Pyrochlore zirconium gadolinium oxide nanorods composite membrane for suppressing the formation of free radical in PEM fuel cell operating under dry condition. *ACS Sustain Chem Eng*. 2019; 7(19):16889-16899.
29. Tsipoaka M, Aziz MA, Park J, Shanmugam S. Ti₂Zr₂O₈ nanotube as an additive in the fuel cell membrane and catalyst layer for improved low humidity operation. *J Power Sources*. 2021; 509:230386.
30. Wang L, Advani SG, Prasad AK. Degradation reduction of polymer electrolyte membranes using CeO₂ as a free-radical scavenger in catalyst layer. *Electrochim Acta*. 2013;109:775-780.
31. Coms FD, Liu H, Owejan JE. Mitigation of perfluorosulfonic acid membrane chemical degradation using cerium and manganese ions. *ECS Trans*. 2008;16(2):1735-1747.
32. Coms FD, Gittleman CS. Stabilization of PFSA membranes using Ce³⁺ and Mn²⁺ redox scavengers: mechanisms and applications. *The Chemistry of Membranes Used in Fuel Cells: Degradation and Stabilization*. Hoboken, NY: John Wiley & Sons; 2017:75-106.
33. Eriksson P, Tal AA, Skallberg A, et al. Cerium oxide nanoparticles with antioxidant capabilities and gadolinium integration for MRI contrast enhancement. *Sci Rep*. 2018;8(1): 6999.
34. Celardo I, Pedersen JZ, Traversa E, Ghibelli L. Pharmacological potential of cerium oxide nanoparticles. *Nanoscale*. 2011;3(4): 1411-1420.
35. Tinh VDC, Kim D. Enhancement of oxidative stability of PEM fuel cell by introduction of HO• radical scavenger in nafion ionomer. *J Membr Sci*. 2020;613:118517.
36. Pearman BP, Mohajeri N, Brooker RP, et al. The degradation mitigation effect of cerium oxide in polymer electrolyte membranes in extended fuel cell durability tests. *J Power Sources*. 2013;225:75-83.
37. Ketpang K, Oh K, Lim S-C, Shanmugam S. Nafion-porous cerium oxide nanotubes composite membrane for polymer electrolyte fuel cells operated under dry conditions. *J Power Sources*. 2016;329:441-449.
38. Baker AM, Mukundan R, Spornjak D, et al. Cerium migration during PEM fuel cell accelerated stress testing. *J Electrochem Soc*. 2016;163(9):F1023-F1031.
39. Banham D, Ye S, Cheng T, et al. Effect of ceox crystallite size on the chemical stability of ceox nanoparticles. *J Electrochem Soc*. 2014;161(10):F1075-F1080.
40. Mittal VO, Kunz HR, Fenton JM. Is H₂O₂ involved in the membrane degradation mechanism in PEMFC? *Electrochem Solid St*. 2006;9(6):A299.
41. Jiang R, Mittelsteadt CK, Gittleman CS. Through-plane proton transport resistance of membrane and ohmic resistance distribution in fuel cells. *J Electrochem Soc*. 2009;156(12):B1440.

42. Soboleva T, Xie Z, Shi Z, Tsang E, Navessin T, Holdcroft S. Investigation of the through-plane impedance technique for evaluation of anisotropy of proton conducting polymer membranes. *J Electroanal Chem.* 2008;622(2):145-152.
43. Schlick S, Danilczuk M, Drews AR, Kukreja RS. Scavenging of hydroxyl radicals by ceria nanoparticles: effect of particle size and concentration. *J Phys Chem C.* 2016;120(12):6885-6890.
44. Munusamy P, Sanghavi S, Varga T, Suntharampillai T. Silica supported ceria nanoparticles: a hybrid nanostructure to increase stability and surface reactivity of nano-crystalline ceria. *RSC Adv.* 2014;4(17):8421-8430.
45. Xue Y, Chan S. Layer-by-layer self-assembly of CHI/PVS-nafion composite membrane for reduced methanol crossover and enhanced DMFC performance. *Int J Hydrogen Energy.* 2015;40(4):1877-1885.
46. Sigwadi R, Dhlamini MS, Mokrani T, Nemavhola F, Nonjola PF, Msomi PF. The proton conductivity and mechanical properties of Nafion[®]/ZrP nanocomposite membrane. *Heliyon.* 2019;5(8):e02240.
47. Krishnamurthy P, Krishnan R, Kaveripatnam Samban D. Performance of a 1 kW class nafion-PTFE composite membrane fuel cell stack. *Int J Chem Eng.* 2012;2012:1-7.
48. Jha SK, Kumar CN, Raj RP, Jha NS, Mohan S. Synthesis of 3D porous CeO₂/reduced graphene oxide xerogel composite and low level detection of H₂O₂. *Electrochim Acta.* 2014;120:308-313.
49. Lu J. Mesoporous nafion membranes for fuel cell applications. *ECS Trans.* 2011;41(1):1555-1560.
50. Mollá S, Compañ V. Polyvinyl alcohol nanofiber reinforced nafion membranes for fuel cell applications. *J Membr Sci.* 2011;372(1-2):191-200.
51. de Bruijn FA, Dam VAT, Janssen GJM. Review: durability and degradation issues of PEM fuel cell components. *Fuel Cells.* 2008;8(1):3-22.
52. Escobedo G, Raiford K, Nagarajan GS, Schwiebert KE. Strategies for mitigation of PFSA polymer degradation in PEM fuel cells. *ECS Trans.* 2006;1(8):303-311.
53. Healy J, Hayden C, Xie T, et al. Aspects of the chemical degradation of PFSA ionomers used in PEM fuel cells. *Fuel Cells.* 2005;5(2):302-308.
54. Schulze M, Lorenz M, Wagner N, Gülzow E. XPS analysis of the degradation of nafion. *Fresenius' J Anal Chem.* 1999;365(1-3):106-113.
55. Chen C, Levitin G, Hess DW, Fuller TF. XPS investigation of Nafion[®] membrane degradation. *J Power Sources.* 2007;169(2):288-295.
56. Huang C, Seng Tan K, Lin J, Lee Tan K. XRD and XPS analysis of the degradation of the polymer electrolyte in H₂-O₂ fuel cell. *Chem Phys Lett.* 2003;371(1-2):80-85.
57. Chastain J, King RC Jr. *Handbook of X-Ray Photoelectron Spectroscopy.* Vol 40. Eden Prairie, MN: Perkin - Elmer Corporation; 1992:221.
58. Vijayakumar M, Bhuvaneshwari MS, Nachimuthu P, et al. Spectroscopic investigations of the fouling process on nafion membranes in vanadium redox flow batteries. *J Membr Sci.* 2011;366(1-2):325-334.
59. Hoffmann EA, Fekete ZA, Korugic-Karasz LS, Karasz FE, Wilusz E. Theoretical and experimental X-ray photoelectron spectroscopy investigation of ion-implanted nafion. *J Polym Sci Part A.* 2004;42(3):551-556.

SUPPORTING INFORMATION

Additional supporting information may be found in the online version of the article at the publisher's website.

How to cite this article: Kang YS, Jang S, Choi E, Jo S, Kim SM, Yoo SJ. Sandwich-like Nafion composite membrane with ultrathin ceria barriers for durable fuel cells. *Int J Energy Res.* 2022;46(5):6457-6470. <https://doi.org/10.1002/er.7582>